Arabian Journal for Science and Engineering (2022) 47:3311–3324
https://doi.org/10.1007/s13369-021-06197-z

RESEARCH ARTICLE-ELECTRICAL ENGINEERING

Performance Evaluation of Multilevel Inverter in Variable Speed SEIG-Based Wind Energy System

Sanjay Dewangan[1] · **Shelly Vadhera**[1]

Received: 21 March 2021 / Accepted: 5 September 2021 / Published online: 28 September 2021

Abstract

The indirect vector control (IVC) technique for stand-alone self-excited induction generator (SEIG)-based wind energy system (WES) is presented in this work. IVC regulates the SEIG speed, torque, and DC voltage independently. Further, the proposed technique is analyzed with back-to-back two-level converter such as generator side converter (GSC) and load side converter (LSC) using space vector pulse width modulation (SVPWM) strategy. Two-level and three-level space vector pulse width modulation inverters are used, and the performance comparison between the two schemes is also discussed during step change of wind speed. The three-level inverter exhibits enhancement of SEIG voltage along with current, speed, DC voltage and torque in contrast to those obtained from two-level inverter. IVC for SEIG-based WES is implemented in MATLAB/SIMULINK software, and the experimental environment is set up for 4 kW system.

Keywords Wind energy system · SEIG · Indirect vector control · Multilevel inverter

Abbreviations

ρ	Air density
A	Turbine swept area
R	Length of the blade in meter
V_w	Wind speed
ω_t^*	Mechanical speed of turbine
β	Pitch angle in degree
s	Laplace operator
ω_r	Generator speed
p	Pole pairs
T_e	Torque developed
ω_{sl}	Slip speed
v_{sd}, v_{sq}	Stator voltages
i_{sd}, i_{sq}	Stator currents
i_{rd}, i_{rq}	Rotor currents
i_{sm}	Magnetizing stator current
R_s,R_r	Winding resistances
L_s,L_r	Self-inductances
L_m	Mutual inductance
λ_{sd}, λ_{sq}, λ_{rd}, λ_{rq}	Stator and rotor fluxes
i_{ed}, i_{eq}	Excitation capacitor currents
C_{ed}, C_{eq}	The value of excitation capacitor in $d-q$ axes
θ	Transformation angle
σ	Leakage factor
τ_r	Rotor time constant
GSC	Generator side converter
IVC	Indirect vector control
LSC	Load side converter
MLI	Multilevel inverter
PI	Proportional integral
SEIG	Self-excited induction generator
TLI	Two-level load side inverter
WES	Wind energy system

✉ Sanjay Dewangan
sanjay_6170067@nitkkr.ac.in

Shelly Vadhera
shelly_vadhera@nitkkr.ac.in

[1] Electrical Engineering, National Institute of Technology, Kurukshetra, Haryana, India

1 Introduction

Limited availability of conventional energy sources for example coal, oil, and gas is a major problem. The demand for electricity has increased recently. Fossil fuels are polluting the atmosphere therefore to save the environment, and researchers are focusing on non-conventional energy sources, for example, hydropower, tidal, solar, biomass, and wind [1, 2]. Wind energy is very popular for the production of electricity at a low cost [3, 4]. At the stand-alone sites, small wind turbines are used to provide electricity [5, 6]. In

the wind energy system (WES), various types of the electrical generator are employed for example permanent magnet synchronous generator (PMSG) and SEIG. The advantages of direct drive PMSG are low maintenance requirements, high efficiency, high power density, and gearless operation. But it is expensive and heavier as compared to self-excited induction generators [7].

Therefore, the major electricity contributor is SEIG for remote areas and rural zones where the power grid is not available. SEIG is mostly used for low and medium power generation with the wind energy system. Under on load and no load conditions, the performance of isolated SEIG has been discussed at the variable speed [8–10]. For self-excitation, a self-excited induction generator requires capacitor banks. Capacitor banks are connected to stator terminals which provide reactive power to an induction machine. A major concern is the variation of stator voltage and frequency of SEIG due to variable wind speeds [11]. The electronic load voltage controller has been used in [12] to minimize these types of problems. Static synchronous compensator (STATCOM) is employed at the point of common coupling to supply magnetizing power and regulate the variation of system voltage [13]. Distribution static compensator (DSTATCOM) is employed to provide magnetizing power for controlling the system voltage [14].

Frequency and voltage variations of isolated SEIG are being controlled by adaptive stator current compensator, and it also controls the stator currents at variable speed and balanced/unbalanced loads [15]. The uncontrolled rectifier is employed to convert the AC voltage of the wind-driven induction generator to a DC voltage. The inverter is used to adjust the unity power factor at the load and to track the peak power of the source [16]. Variation of frequency and stator voltage of induction machines are regulated by desired techniques such as scalar control, direct torque control (DTC) and IVC method [17–19].

The scalar control method is utilized to calculate the induction motor speed which has been driven using the inverter with SVPWM strategy [17]. DTC method was utilized to regulate the variation in frequency and voltage of induction generator. DTC has ease in structure but faces the problem of variable switching frequency limitation. DTC with PI controller gives the sluggish response of torque ripples, and flux ripples with settling time [18].

DTC method and vector control technique are employed in [19] at random wind velocity to control the rotor and grid side converter, respectively. Flux ripples, torque ripples, and settling problems are given by the proportional integral (PI) controller. Modern approaches such as an artificial neural network and adaptive neuro-fuzzy inference system were implemented to minimize this difficulty. At variable load and rotor speed, the indirect rotor field oriented (IRFO) controller is implemented in [20] to regulate the DC voltage. IRFO technique is used to regulate the three-phase insulated gate bipolar transistor (IGBT) power converter at variable speed, and the fuzzy logic controller (FLC) approach optimizes the operating flux of SEIG. The main aim is to obtain a constant DC voltage [21]. In [22, 23], a field oriented control approach with two-level inverter (TLI) is employed to regulate voltage and frequency variation of induction machine and torque ripples are also minimized but harmonics present in the current. DTC approach with multilevel inverter (MLI) is implemented to overcome the torque ripples and current distortion of the induction machine [24].

The comparisons have been investigated between MLI and convectional two-level inverter. MLI is used to minimize the total harmonics distortions of voltage, current, and switching losses. It gives better efficiency and power quality [25]. MLI replaces a two-level inverter for power quality improvement. The fuzzy logic pulse generator is used to provide the gate signal which has been discussed in [26]. Performance comparisons between two-level and three-level inverters using SVPWM strategy are discussed in [27] where only a problem of few ripples is present in the transient responses of the system with three-level inverter using DTC technique. Multilevel inverter-fed induction machines are controlled by model predictive torque control using sorting networks [28]. For three-level neutral point clamped driven induction motor drives; model predictive flux control is employed. It has more benefits for example simplicity, fast dynamic response, and multi-objective control [29].

Conventional DTC technique cannot be developed simply for a multilevel inverter because of the high amount of possible voltage vectors existing for choice, but vector control can be naturally be developed for multilevel inverter fed drives using a space vector modulation PWM technique.

Implementing vector control method with multilevel converters for speed control of the motor is fully explored, but still the variable speed operation of induction generator is explored very little. Isolated SEIG-based WES is discussed in [5], where more undershoot/overshoot of SEIG speed, DC link voltage, and sluggish torque response are obtained by indirect vector control technique with two-level inverter using SVPWM strategy.

The independent control of SEIG system is obtained on machine side converter and load side MLI, with the following important contributions:

- The main objective of this work is to achieve quick response in dynamic performance of torque and generator speed.
- The machine side converter is controlled by the IVC technique that enables the stand-alone SEIG-based wind energy system to easily regulate its speed, torque, and flux.

- The load side TLI is replaced by MLI. The MLI along with IVC technique efficiently maintains a constant DC link voltage at variable speeds.
- Bode plot and Root locus are used to analyze the stability of the proposed system.
- Simulation and experimental results shows close proximity and hence validates the successful implementation of MLI in variable speed SEIG.

In a MATLAB/Simulink environment, the simulation results are performed and a prototype model is designed to experimentally verify the performance using the dSPACE DS-1104 R&D controller board. For the first time in the available literature, both simulation and experimental results are discussed in order to verify the IVC technique that gives power with desirable load voltage and frequency at variable speeds.

The paper is organized as follows. The developed scheme is presented in Sect. 2. Section 3 explains the modeling of the wind turbine. The dynamic modeling of generator using the IVC technique is illustrated in Sect. 4. The three-level MLI is described in Sect. 5. The simulation and experimental results are discussed in Sect. 6 for WES.

2 Developed Scheme

Figure 1 elaborates the schematic diagram of the developed stand-alone SEIG-based WES. It consists of a wind turbine, SEIG, generator side converter, load side three-level neutral point clamped inverter, fixed capacitor bank, and resistive-inductive load. A fixed capacitor bank provides leading magnetizing energy to SEIG for maintaining voltage. A prime mover is mechanically coupled with an induction generator through a gear box that can control the turbine speed for the induction generator. Active power is generated by SEIG at above synchronous speed. The proposed system has stability problems such as variation of torque, flux, and DC link voltage during variable speed. To control the variation of system parameters, power converters are used. The generator side converter is controlled by the IVC technique using the proportional integral (PI) controller to calculate the reference torque in an outer speed control loop. The load side two-level inverter (TLI) is utilized to regulate active power and reactive power using an indirect vector control method. Sluggish torque and more undershoot/overshoot of speed are obtained using TLI. In the proposed stand-alone SEIG-based wind energy system, space vector modulation PWM strategy is applied for obtaining better switching pulses. The two-level inverter in the load side of WES is replaced with three-level neutral point clamped MLI to improve the harmonic profile and reduced switching losses. Proposed system can be a bit costlier with three-level inverter, but the proposed IVC technique with a three-level inverter using SVPWM scheme yields better performance at step change of wind speed conditions compared to the existing two-level-inverter-based WES.

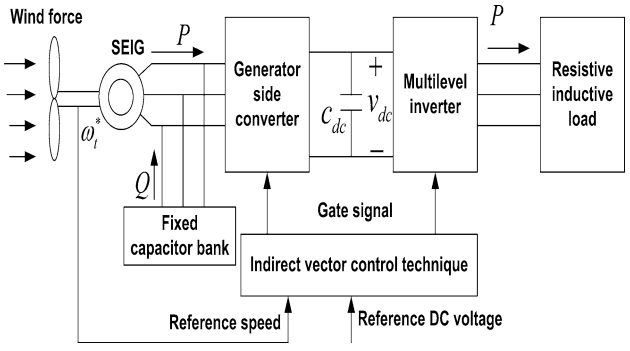

Fig. 1 SEIG-based WES

3 Wind Turbine Modelling

Prime mover torque T_m can be written by,

$$T_m = \frac{1}{2}\rho \mathrm{ARC}_p V_w^2/\lambda \tag{1}$$

where C_p and ω_t are the power coefficient and rotational speed of the prime mover. The tip speed ratio can be described as follows:

$$\lambda = R\omega_t/V_w \tag{2}$$

$$C_p = \frac{1}{2}\left(\frac{116}{\lambda_1} - 0.4 * \beta - 5\right)e^{\frac{-16.5}{\lambda_1}} \tag{3}$$

$$\lambda_1 = \frac{1}{\frac{1}{(\lambda+0.089)} - \frac{0.035}{(\beta^3+1)}}. \tag{4}$$

4 Dynamic Model of SEIG Using IVC

The proposed indirect vector control technique using PI controller schematic diagrams is depicted in Fig. 2.

Dynamic equations have been expressed for the SEIG:

$$\lambda_r = \lambda_{\mathrm{rd}} = -\tau_r \frac{\mathrm{d}}{\mathrm{d}t}\lambda_{\mathrm{rd}} + L_m i_{\mathrm{sd}}, \quad \lambda_{\mathrm{rq}} = 0 \tag{5}$$

$$\lambda_{\mathrm{sd}} = \frac{L_m}{L_r}\lambda_{\mathrm{rd}} + \sigma L_s i_{\mathrm{sd}}, \quad \lambda_{\mathrm{sq}} = \sigma L_s i_{\mathrm{sq}} \tag{6}$$

$$i_{\mathrm{rq}} = -\frac{L_m}{L_r} i_{\mathrm{sq}}, \quad i_{\mathrm{rd}} = \frac{\lambda_{\mathrm{rd}} - L_m i_{\mathrm{sd}}}{L_r} \tag{7}$$

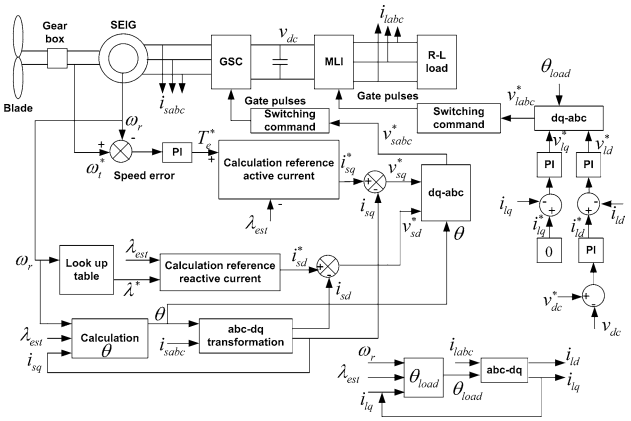

Fig. 2 SEIG using indirect vector control

$$v_{\mathrm{sd}} = R_s i_{\mathrm{sd}} + \sigma L_s \frac{\mathrm{d}i_{\mathrm{sd}}}{\mathrm{d}t} - \omega_e \sigma L_s i_{\mathrm{sq}} + \frac{1}{\tau_r}\left(-\frac{L_m}{L_r}\lambda_{\mathrm{rd}} + \frac{L_m^2}{L_r} i_{\mathrm{sd}}\right) \tag{8}$$

$$v_{\mathrm{sq}} = R_s i_{\mathrm{sq}} + \sigma L_s \frac{\mathrm{d}i_{\mathrm{sq}}}{\mathrm{d}t} + \omega_e \sigma L_s i_{\mathrm{sd}} + \omega_e \frac{L_m}{L_r}\lambda_{\mathrm{rd}} \tag{9}$$

The torque T_e is followed by

$$T_e = -\frac{3p}{4}\left(\omega_e L_m i_{\mathrm{sm}} i_{\mathrm{sq}}\right) \tag{10}$$

The slip speed is presented by

$$\omega_{\mathrm{sl}} = \left(\frac{1}{\tau_r}\right)\left(\frac{L_m}{\lambda_{\mathrm{rd}}}\right) i_{\mathrm{sq}} \tag{11}$$

where $\tau_r = \left(L_r/R_r\right)$.

4.1 Design PI Speed Control Loop

Figure 3 discusses the PI controller speed control loop. The simplified model is made by Eqs. (5) and (9). The transfer function has been calculated by the nominal WES model using Fig. 3.

$$\frac{\omega_r(s)}{\omega_t^*(s)} = \sqrt{\frac{3}{2}}\frac{\omega_e L_m^2 k_{\mathrm{ii}}}{\tau_r L_r}\frac{\left(T_i s + 1\right)}{\left(s^2 + 2\xi_i \omega_{\mathrm{ni}} s + \omega_{\mathrm{ni}}^2\right)} \tag{12}$$

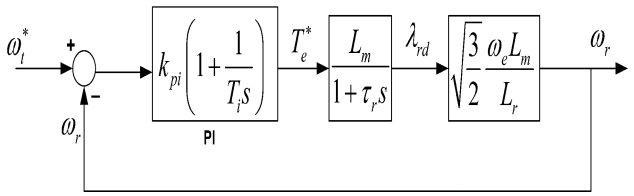

Fig. 3 PI controller speed control loop for GSC

PI controller parameters are described by

$$k_{\mathrm{pi}} = \sqrt{\frac{2}{3}}\frac{L_r}{\omega_e L_m^2}\left(2\xi_i \tau_r \omega_{\mathrm{ni}} - 1\right), \quad T_i = \frac{k_{\mathrm{pi}}}{k_{\mathrm{ii}}} = \frac{\left(2\xi_i \tau_r \omega_{\mathrm{ni}} - 1\right)}{\tau_r \omega_{\mathrm{ni}}^2}$$

Unit step response of Eq. (12) has been written with $\xi = \sqrt{2}/2$ damping ratio,

$$\omega_r(t) = 1 - \frac{1}{\sqrt{(1-\xi_i^2)}} e^{-\xi_i \omega_{\mathrm{ni}} t} \left[\left(-\xi_i + \frac{1}{\tau_r \omega_{\mathrm{ni}}}\right)\sin(\omega_{\mathrm{ni}}\sqrt{1-\xi_i^2}\,t) + \sqrt{1-\xi_i^2}\cos(\omega_{\mathrm{ni}}\sqrt{1-\xi_i^2}\,t)\right] \tag{13}$$

The desired tracking specification with response time is obtained by the PI controller using Eq. (13) and solving the above mathematical equation to achieve natural frequency ω_{ni}. Using the parameters $\tau_r = 0.113$ s and $L_m = 0.0061$ H, at the full load and rated speed $\omega_e = 149.75$ rad/s with setting t_{re} responses time to 0.07 s, the parameters of PI controller are $k_{\mathrm{pi}} = 0.061$, $k_{\mathrm{ii}} = 1.26$ and integral time $T_i = 0.0485$ s where $\omega_{\mathrm{ni}} = 20$ rad/s.

Figure 4 shows for the SEIG speed with PI controller, the open loop bode editor and root locus editor. Proposed system is stable because of poles and zero are in left-hand side of zero value. The stability of the Eq. (12) has been examined by SISOTOOL which has been implemented in MATLAB.

4.2 Modelling of Excitation Capacitor

Excitation capacitor dynamic equations have been presented by direct-quadrature axis component of generator voltage as state variables, presented by the following:

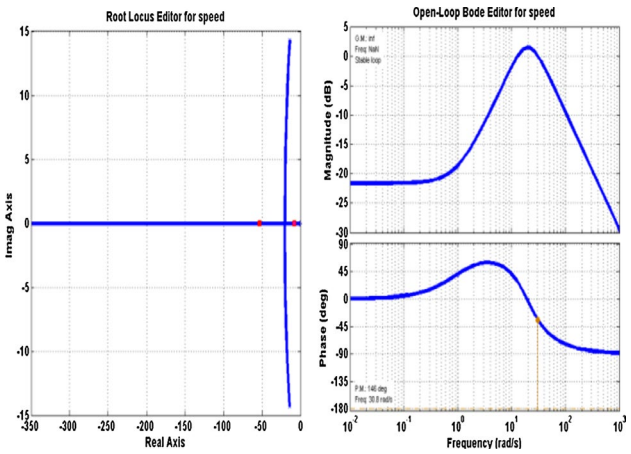

Fig. 4 Root locus editor and open loop bode editor for speed

$$\frac{\mathrm{d}v_{\mathrm{sd}}}{\mathrm{d}t} = \frac{i_{\mathrm{ed}}}{C_{\mathrm{ed}}}, \tag{14}$$

$$\frac{\mathrm{d}v_{\mathrm{sq}}}{\mathrm{d}t} = \frac{i_{\mathrm{eq}}}{C_{\mathrm{eq}}}. \tag{15}$$

Two variables are transformed into three variables which have been presented by generator three-phase voltages equations

$$v_a = 0.v_{\mathrm{sd}} + 1.v_{\mathrm{sq}} \tag{16}$$

$$v_b = -\frac{\sqrt{3}}{2}v_{\mathrm{sd}} - \frac{1}{2}v_{\mathrm{sq}} \tag{17}$$

$$v_c = \frac{\sqrt{3}}{2}v_{\mathrm{sd}} - \frac{1}{2}v_{\mathrm{sq}} \tag{18}$$

5 Neutral Point Clamped Three-Level Inverter

In the wind energy system, the multilevel inverter can be employed to change from DC to AC voltage. Generator speed, the DC voltage, active power, and reactive power are system parameters that need to be regulated. The torque and flux variations are regulated by the generator side converter. Reactive power and active power variations are controlled by load side multilevel inverter using the SVPWM strategy. Figure 5 depicts the three-level neutral point clamped inverter.

Four switches S_1, S_2, S_3, S_4 with four anti-parallel diodes D_1, D_2, D_3, D_4 are available in the inverter leg A. The DC bus capacitor has been divided into two capacitors on the DC side that makes a neutral point Z. The clamping diodes are D_{Z1} and D_{Z2} that have been connected to the neutral point. The output terminal A of the inverter is connected to the neutral point using one of the clamping diodes when switches S_2 and S_3 are turned on. The voltage across each of the DC capacitors is E, which is normally equal to $v_{\mathrm{dc}}/2$. Neutral current i_Z charges or discharges the capacitors C_{d1} and C_{d2}, causing neutral point voltage deviation.

5.1 Space Vector Pulse Width Modulation

For power electronics applications, space vector PWM strategy is being implemented to minimize harmonic content, switching losses and develop the power quality. Reference vector V_{ref} represents a three-phase voltage which rotates at an angular speed $2\pi f$. The reference vector V_{ref} is generated

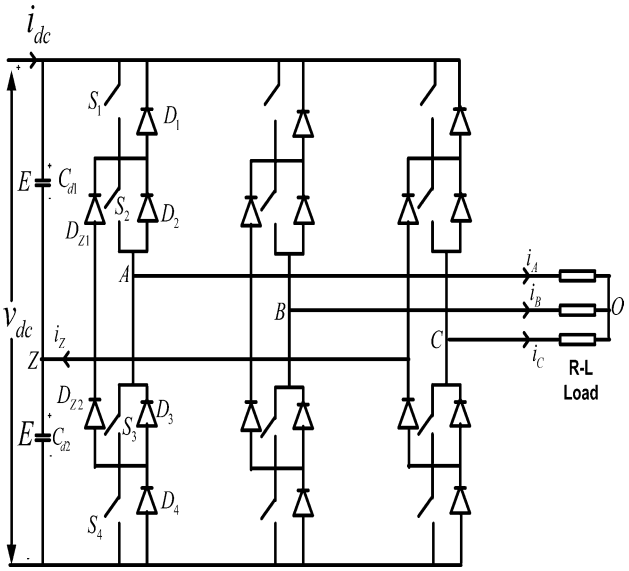

Fig. 5 Three-level inverter

Table 1 Description of switching states

Switching state	Device switching state (Phase A)				Inverter terminal voltage v_{AZ}
	S_1	S_2	S_3	S_4	
P	On	On	Off	Off	E
O	Off	On	On	Off	0
N	Off	Off	On	On	$-E$

by correctly selecting the various combinations of switching states.

5.2 Switching States

Table 1 tabulates the switching states where switching state 'P' represents that the above two switches in leg A are on, the inverter terminal voltage v_{AZ} exhibits that the voltage at terminal A with respect to the neutral point Z is $+E$, but 'N' exhibits that the below two switches conduct, leading to $v_{\mathrm{AZ}} = -E$, switching state 'O' denotes that the middle two switches S_2 and S_3 are on and $v_{\mathrm{AZ}} = 0$.

The process of turning on one of the two clamping diodes depends on the direction of load current. For instance, clamping diode is turned on by a positive load current ($i_A > 0$), and the neutral point Z is connected to the terminal A through the conduction of S_2 and D_{Z1}. Switches S_1 and S_3 are operated in a complementary manner. Similarly, S_2 and S_4 are a complementary pair. The three-level inverter has three voltage levels, $+E$, 0, and $-E$ for the waveform of v_{AZ}. Line-to-line (L-L) voltage waveform is found which is depicted in Fig. 6. The inverter terminal

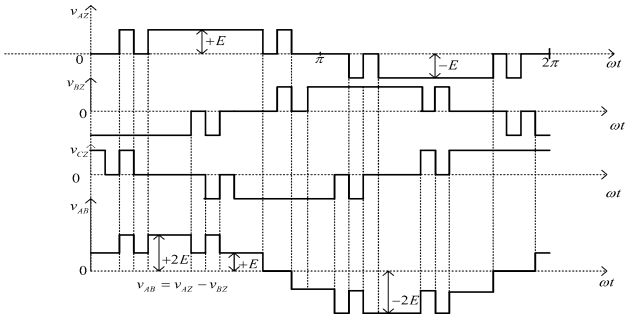

Fig. 6 Inverter L-L voltage

voltages v_{AZ}, v_{BZ}, and v_{CZ} are three phase balanced with a phase shift of 2π/3 between each other. The L-L voltage v_{AB} is obtained from $v_{AB} = v_{AZ} - v_{AZ}$, which contains five voltage levels $(+2E, +E, 0, -E, and -2E)$.

5.3 Stationary Space Vectors

The three switching states [P], [O], and [N] denote the working of each inverter phase leg. The inverter has a total of 27 switching states. Figure 7 illustrates the space vector diagram of the 19 voltage vectors. Voltage vectors have been separated into four groups based on their magnitude: (i) Three switching states [PPP], [OOO], and [NNN] are represented by zero vector (V_0), and the magnitude of V_0 is zero. (ii) The vectors from V_1 to V_6 are known as small vectors which have a magnitude of $v_{dc}/3$ for each. Two switching states are available for each of these vectors. The vector one containing [P] and the other containing [N], because of, it has been further divided into a P or N type small vector. (iii) The vector from V_7 to V_{12} are known as medium vectors with the magnitude of $\sqrt{3}v_{dc}/3$. (iv) The vectors from V_{13} to V_{18} are known as large vectors with the magnitude of $2v_{dc}/3$.

5.4 Dwell Time Calculation

Six triangular sectors (I to VI) are made by the space vector diagram to determine the dwell time. Each sector has been further separated into four triangular regions (1 to 4) as described in Fig. 8. The SVPWM technique has been similarly used for the two-level inverter. The SVPWM technique bases on the "volt-second balancing" principle; that is, the product of the reference voltage V_{ref} and sampling period T_s equals the sum of the voltage multiplied by the time interval of selected space vectors. The reference vector V_{ref} is synthesized by three nearest stationary vectors in the three-level inverter.

For instance, when V_{ref} drops into zone 2 of sector I, the three nearest vectors V_1, V_2, and V_7, from which

$$V_1 T_a + V_7 T_b + V_2 T_c = V_{ref} T_s \tag{19}$$

Here $T_a + T_b + T_c = T_s$, where T_a, T_b, and T_c are the dwell times for V_1, V_7, and V_2, respectively. Vector V_{ref} is synthesized by other space vectors instead of the three nearest vectors.

5.5 Switching Sequence with Minimal Neutral Point Voltage Deviation

The neutral point voltage v_Z is increased due to P-type small vector but an N-type small vector drops v_Z. The dwell time of a provided small vector is equally provided between the P- and N-type switching states over a sampling period to reduce the neutral point voltage deviation. The reference vector $\vec{V}_{ref}$ lies in the triangular zone, and two cases can be tested. When the reference vector $\vec{V}_{ref}$ is in zone 3 or 4 of the sector I, only one of the three selected vectors is the small vector. Vectors $\vec{V}_2$, $\vec{V}_7$, and $\vec{V}_{14}$ are used to synthesize the reference vector $\vec{V}_{ref}$ which drops into zone 4. [PPO] and [OON] are two switching states for the

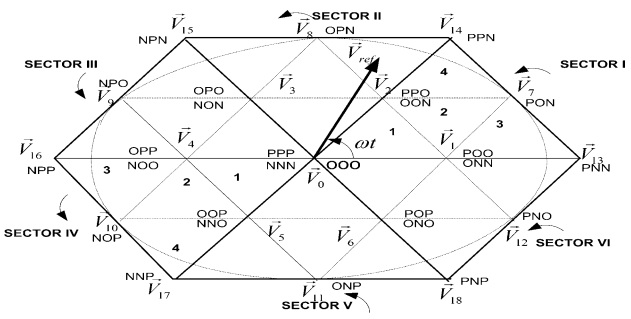

Fig. 7 Division of sectors

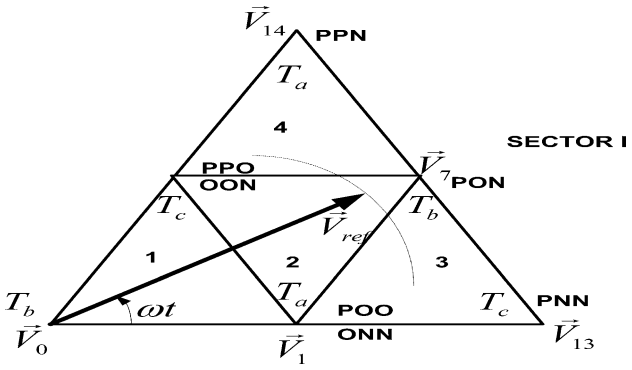

Fig. 8 Four triangular regions of sector I

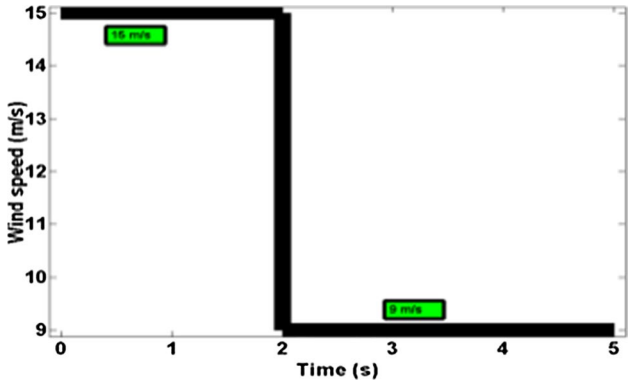

Fig. 9 Wind speed

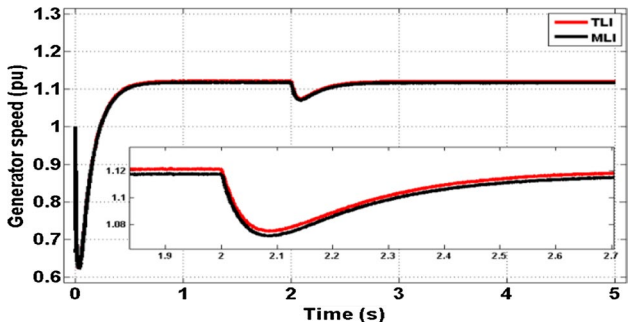

Fig. 10 Generator speed using TLI and MLI

small vector $\vec{V}_2$. The dwell time for $\vec{V}_2$ has been equally given between the two states P and N type.

6 Evaluation

6.1 Simulation Results

Indirect vector control (IVC) using a two-level (TLI) and three-level inverters (MLI)-based wind energy system has been operated at a step change of wind speed. Various components of SEIG, reactive power, DC voltage and load line voltage have been illustrated to validate the system operation. The initial speed of the wind is taken as 15 m/s then and changed to 9 m/s at t = 2 s, as discussed in Fig. 9.

6.1.1 Generator Speed Response

The response of generator speed is captured in Fig. 10. The reference speed has been taken 1.117 pu. At $t = 2$ s, IVC with two-level inverter delivers SEIG speed undershoot of 4.57% and settles within 0.73 s, but IVC with three-level inverter yields speed undershoot 4% and has the settling time of 0.6 s.

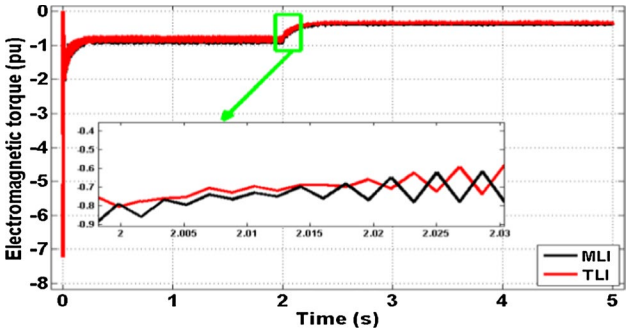

Fig. 11 Torque with TLI and MLI

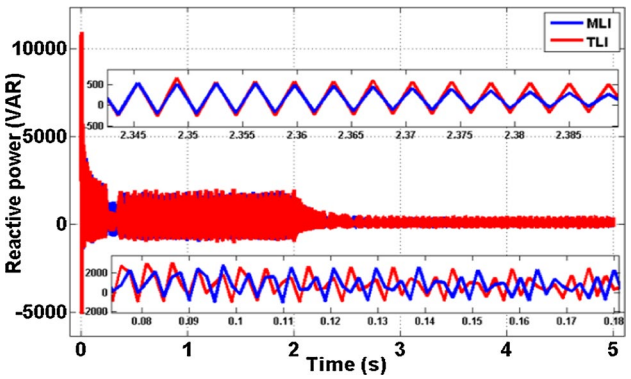

Fig. 12 Reactive power with TLI and MLI

6.1.2 Torque Variation

Electromagnetic torque response is illustrated in Fig. 11. The reference torque is to be taken −0.8 pu. At instant of $t = 2$ s, IVC with two-level inverter delivers torque overshoot of 2.7% and settles within 0.74 s, but IVC with three-level inverter yields torque overshoot of 1.33% and has settling time of 0.69 s.

6.1.3 Reactive Power Response

Figure 12 depicts the response of reactive power. During 15 m/s wind velocity, IVC with two-level inverter is giving the oscillations of reactive power between −950 and 1850 VAR, but IVC with three-level inverter yields ranges between −550 and 1650 VAR. At 9 m/s wind velocity, IVC with two-level inverter is giving the oscillations of reactive power between −200 and 410 VAR, but IVC with three-level inverter shows variation only between −180 and 390 VAR.

6.1.4 Active Power Response

The generated active power response is illustrated in Fig. 13. In this, the highlighted portion is plotted during the time

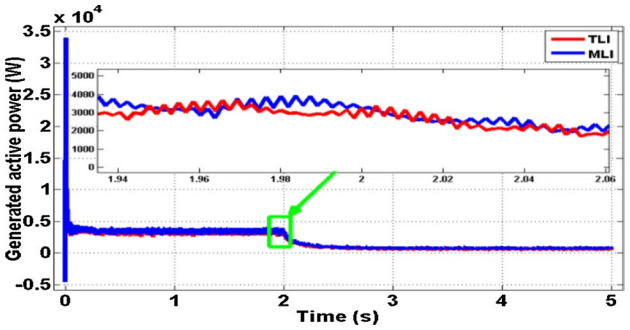

Fig. 13 Generated active power with TLI and MLI

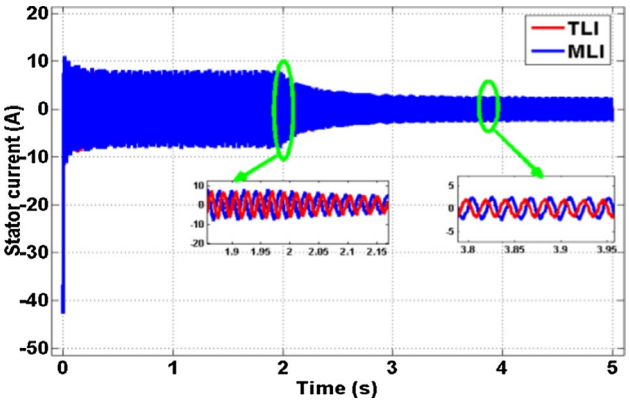

Fig. 14 Stator current with TLI and MLI

$t = 1.94$ to 2.06 s. The power generated for IVC with a two-level inverter is 91% of its rated power, but IVC with three-level inverter exhibits the active power to be 96% of its rated power during 15 m/s wind velocity. At instant of $t = 2$ s, IVC with two-level inverter is giving power undershoot of 31.25% which settles within 0.72 s, but IVC with three-level inverter yields undershoot of 17.5% and settles within 0.61 s.

6.1.5 Current and Voltage Response

The response of the SEIG current is shown in Fig. 14. At maximum wind speed, IVC with a two-level inverter is giving the SEIG current oscillations between −7.2 and 7.2 A, but the proposed IVC with three-level inverter delivers between −8 and 8 A which is nearer to its rated current. When the wind speed is minimum, IVC with a two-level inverter is giving the stator current oscillations between −2.09 and 2.09 A, but IVC with a three-level inverter delivers between −2.6 and 2.6 A. TLI is giving total harmonics distortions (THD) of 7.41%, but MLI yields 6.06% which is given in Figs. 15 and 16, respectively. Figure 17 projects the SEIG phase A voltage. At maximum wind speed, IVC with a two-level inverter is giving the SEIG

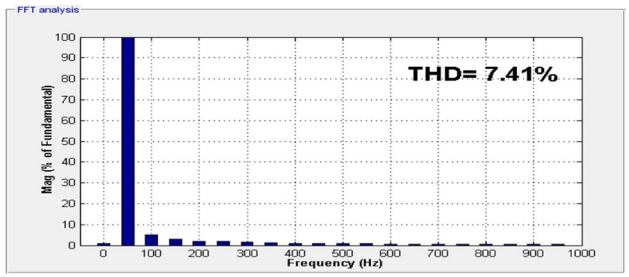

Fig. 15 THD % of stator current with TLI

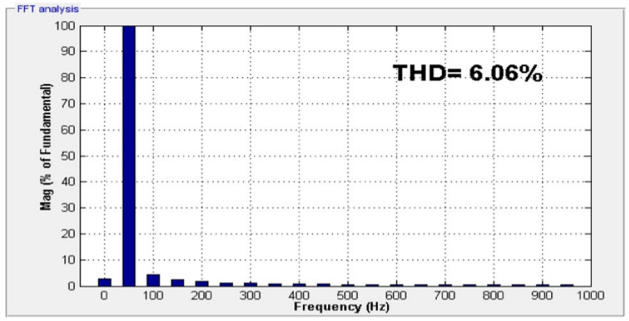

Fig. 16 THD % of stator current with MLI

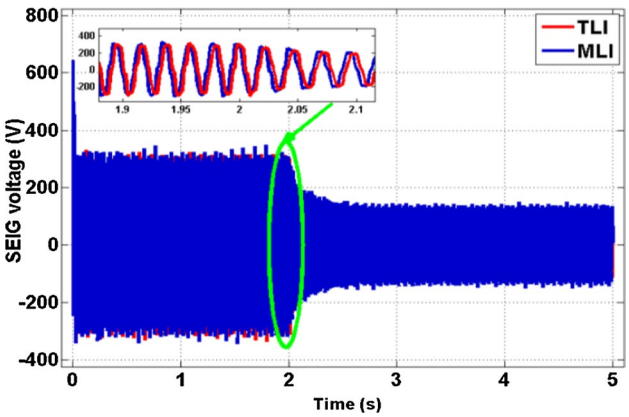

Fig. 17 SEIG voltage with TLI and MLI

voltage oscillations between −323 and 323 V, whereas the proposed IVC with three-level inverter delivers between −324 and 324 V which is nearer to its rated voltage. During lowest wind speed, IVC with a two-level inverter delivers the SEIG voltage oscillations between −118 and 118 V, but the IVC with three-level inverter has the range between −136 and 136 V. Total harmonics distortions for TLI and MLI are 4.95% and 2.95%, respectively, as depicted in Figs. 18 and 19.

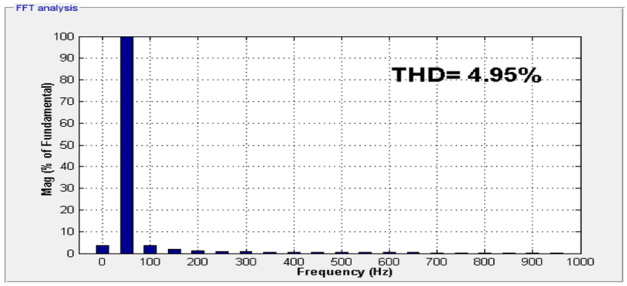

Fig. 18 THD % of SEIG voltage with TLI

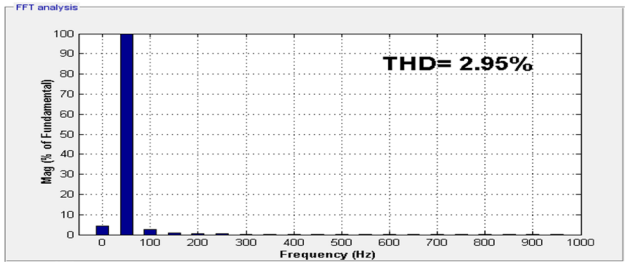

Fig. 19 THD % of SEIG voltage with MLI

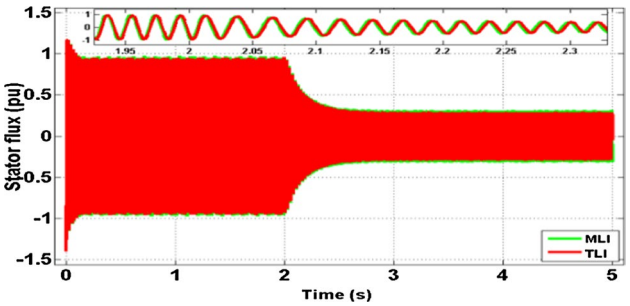

Fig. 20 Stator flux with TLI and MLI

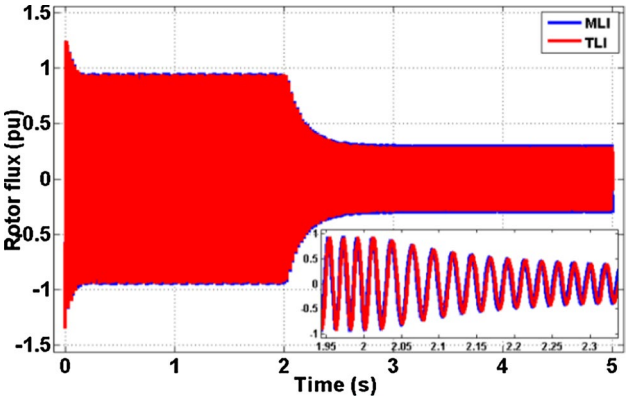

Fig. 21 Rotor flux with TLI and MLI

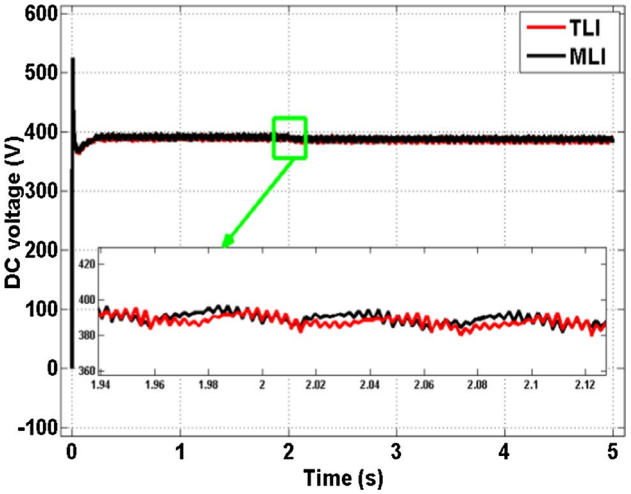

Fig. 22 DC voltage with TLI and MLI

6.1.6 Stator and Rotor Flux Response

When the wind speed is changed from maximum to minimum at instant of $t = 2$ s, stator flux reduces. IVC with two-level inverter delivers stator maximum flux of 0.93 pu, but IVC with three-level inverter has peak flux 0.95 pu at maximum wind speed. Stator flux variation is illustrated in Fig. 20. Figure 21 demonstrates the response of rotor flux. Rotor peak flux has been achieved 0.925 pu with IVC using a two-level inverter, but IVC using three-level inverter yields rotor peak flux of 0.952 pu during 15 m/s of wind speed.

6.1.7 DC Voltage Response

DC voltage response is explained in Fig. 22 with the zoom view from the time $t = 1.94$ to 2.12 s. Reference DC voltage is selected to be 400 V. At instant of $t = 2$ s, IVC with two-level inverter delivers DC voltage undershoot of 1.75% settles within 0.70 s but, IVC with three-level inverter gives undershoot 1.25% and has the settling time of 0.62 s.

6.1.8 Variation in Load Active Power

The load active power variation with variable wind velocity operation is illustrated in Fig. 23. In this, the zoom portion is plotted during the time $t = 1.9$ to 2.06 s. The load active power obtained for TLI-based WES at maximum wind velocity is 90% of its rated power, but MLI yields the load active power 95% of its rated power. At the time 2 s, TLI is giving power undershoot 9.5% and settle at $t = 0.76$ s, but MLI yields undershoot 6.2% and settle at $t = 0.63$ s.

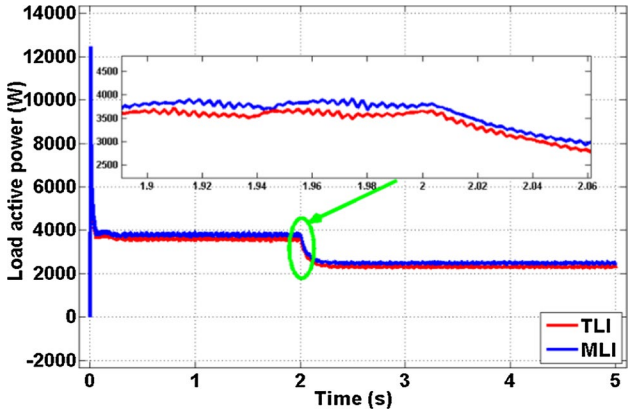

Fig. 23 Load active power with TLI and MLI

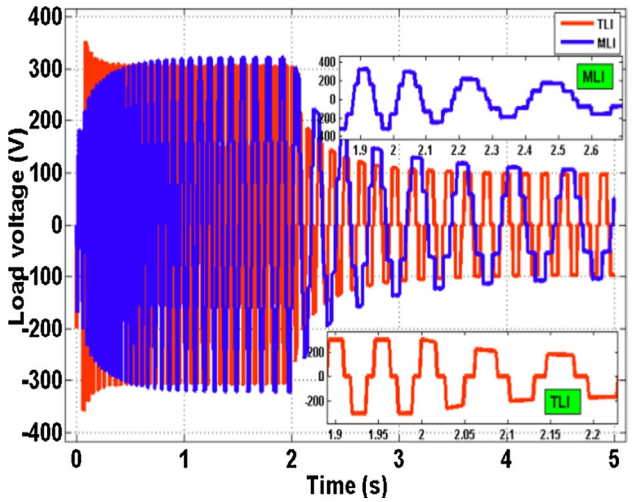

Fig. 24 Load voltage with TLI and MLI

Fig. 25 Test system of SEIG-based WES

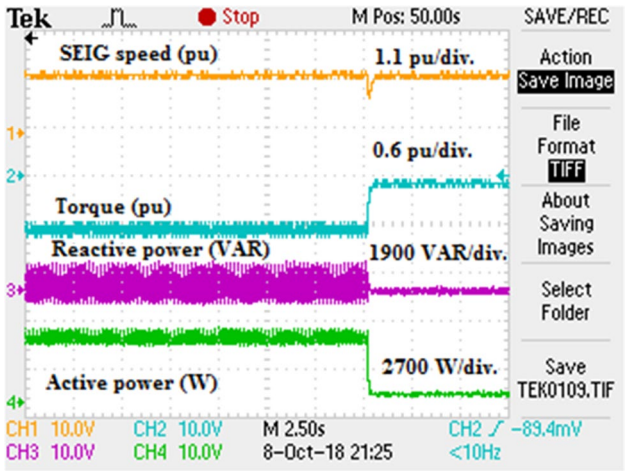

Fig. 26 SEIG speed, torque, reactive power, and active power with TLI

6.1.9 Load voltage Variation

Figure 24 describes the load line voltage at variable wind velocity with TLI and MLI based WES. When wind velocity is maximum, the load line voltage is oscillated between −307 and 307 V for TLI, and the proposed MLI yields between −321 and 321 V which is nearer its rated voltage. At lowest wind speed, the load line voltage oscillates between −102 and 102 V with TLI, but the MLI yields the range between −118 and 118 V. Hence, MLI is better than TLI.

6.2 Experimental Results

6.2.1 Test system

In the laboratory, a prototype of the 4 kW SEIG-based WES is developed. In Fig. 25, the power module is utilized to control the SEIG speed, electromagnetic torque, and DC voltage independently using an indirect vector control method. DC motor is coupled to a rotor of SEIG. A fixed capacitor bank has been connected to SEIG terminals to give reactive power and to obtain the rated voltage at rated speed. For voltage production and stabilization, the magnetizing reactance variation is an important factor. Voltage sensors are used to measure the three-phase voltages and current sensors are implemented for measuring the line currents. The actual speed of the machine is measured by an encoder. SVPWM scheme has been implemented for producing gate signals using the dSPACE DS1104 R&D controller board to regulate generator side converter and load side MLI. The control algorithm is processed with a sample time of 60 μs.

6.2.2 Response of SEIG Speed

Figures 26 and 27 depict the experimental dynamic response of the speed, torque, reactive power, and active power. There

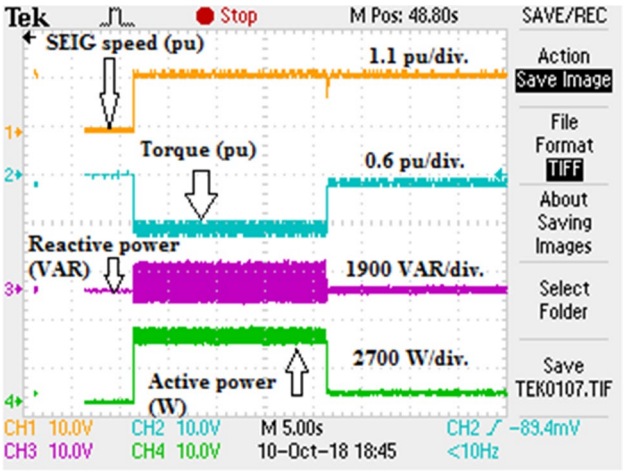

Fig. 27 SEIG speed, torque, reactive power, and active power with MLI

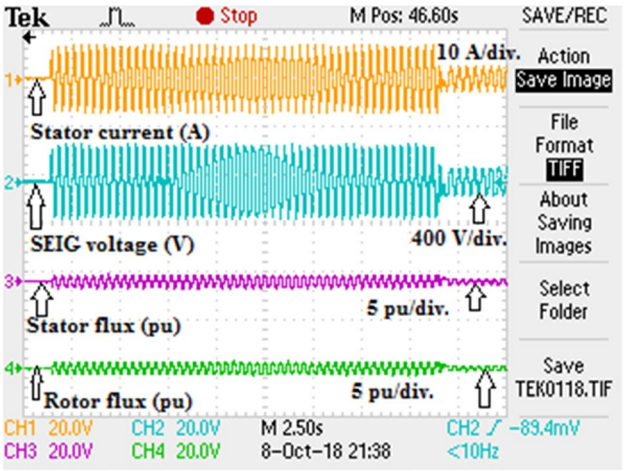

Fig. 28 Generator current, voltage, stator flux, and rotor flux with TLI

parameters are tuned in channels 1, 2, 3, and 4 with IVC using two-level and three-level inverters respectively.

The reference speed is 1.117 pu. The response of SEIG speed is captured in channel 1. At instant $t=2$ s, wind velocity is changed from 15 to 9 m/s and then IVC with a two-level inverter delivers generator speed undershoot of 6% and settles within 0.75 s, but IVC with a three-level inverter has undershoot of 5% and settles within 0.62 s. Therefore, SEIG speed is more near the reference speed using IVC with a three-level inverter.

6.2.3 Torque Variation

Channel 2 describes the torque variations. The reference torque is taken as −0.8 pu. At $t=2$ s, due to wind speed variation, IVC with two-level inverter shows torque overshoot of 3% and settles by 0.77 s, but IVC with three-level inverter yields torque overshoot of 2% and settles by 0.71 s. It has been also investigated that the IVC with a three-level inverter-based system is giving a few disturbances and smooth responses as compared to IVC with a two-level inverter-based system.

6.2.4 Reactive Power Response

The reactive power response is framed in channel 3. At maximum wind velocity of 15 m/s, IVC with two-level inverter delivers the oscillations of reactive power between −960 and 1860 VAR, but IVC with three-level inverter shows between −560 and 1660 VAR. At minimum wind velocity of 9 m/s, IVC with two-level inverter has the reactive power variations between −210 and 420 VAR, whereas the IVC with three-level inverter has a range between −190 and 400 VAR and hence emphasizes a better response.

6.2.5 Active Power Response

The generated active power response is taken on Channel 4. At maximum wind velocity of 15 m/s, active power has been obtained to be of 92% using IVC with two-level inverter, but the proposed IVC with three-level inverter provides the active power 97% of its rated power. At $t=2$ s, wind speed has been reduced from 15 to 9 m/s, in IVC with two-level inverter, the undershoot is of 32% and settles within 0.72 s, but in IVC with three-level inverter, the undershoot is of 18% and settles within 0.64 s.

6.2.6 Current and Voltage of Phase A in SEIG

The experimental dynamic response of SEIG current, output terminal voltage, stator flux, and rotor flux is captured by channels 1, 2, 3, and 4 with IVC using two-level and three-level inverters, respectively, in Figs. 28 and 29. SEIG phase A current response is taken at channel 1. At 15 m/s of wind speed, IVC with two-level inverter gives the SEIG current oscillations between −7.5 and 7.5 A with more settling time 0.73 s, but the proposed IVC with three-level inverter delivers variations between −8.03 and 8.03 A with less settling time 0.62 s. Moreover, at minimum wind velocity of 9 m/s, IVC with two-level inverter has the stator current oscillations between −2.1 and 2.1 A with more settling time 0.68 s, but IVC with three-level inverter it delivers variations between −2.9 and 2.9 A with less settling time 0.58 s. It is investigated from Figs. 30 and 31 that the total harmonics distortions (THD) are of 9.3% and 7.2%, when using IVC with two-level and three-level inverters, respectively.

The generator voltage variation is described in Channel 2. At maximum wind speed of 15 m/s, IVC with a two-level inverter shows output terminal voltage oscillations between

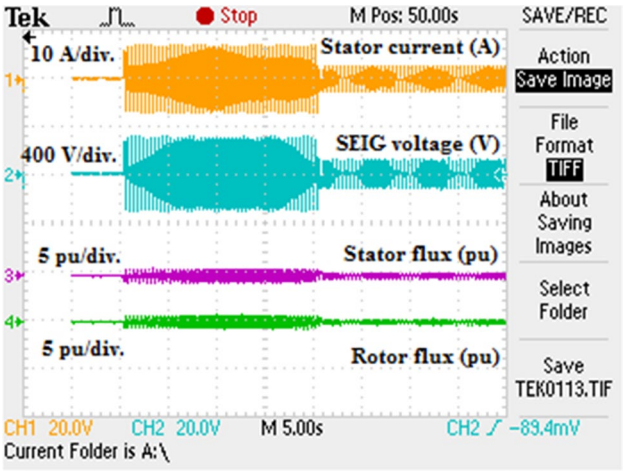

Fig. 29 Generator current, voltage, stator flux and rotor flux with MLI

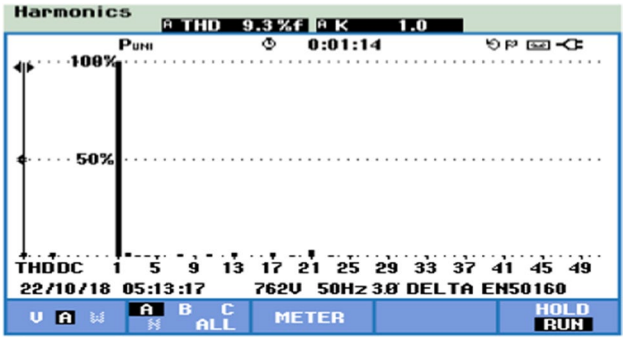

Fig. 30 THD % of stator current with TLI

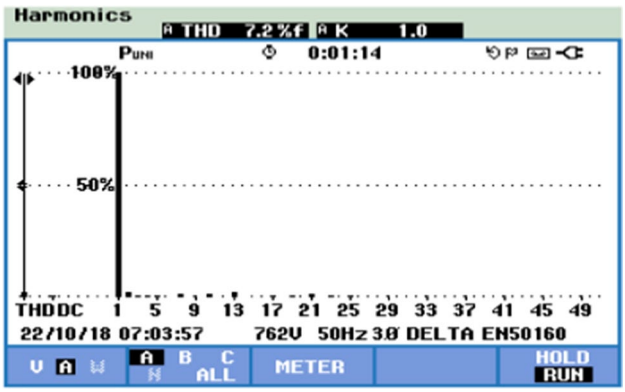

Fig. 31 THD % of SEIG current with MLI

-324 to 324 V with more settling time 0.74 s; however, using the proposed IVC with a three-level inverter the oscillations are between −325 and 325 V with less settling time 0.68 s

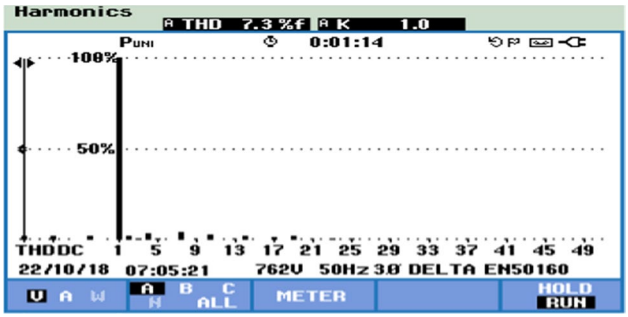

Fig. 32 THD % of SEIG voltage with TLI

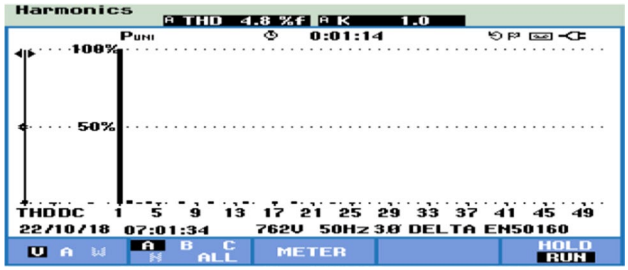

Fig. 33 THD % of SEIG voltage with MLI

which are nearer to its rated voltage. During the minimum wind velocity of 9 m/s, IVC with two-level inverter gives output voltage profile oscillations between −119 and 119 V with more settling time 0.69 s, but the IVC with three-level inverter the range is between −137 and 137 V with less settling time 0.59 s. From Figs. 32 and 33, it has been investigated that the total harmonics distortions (THD) are 7.3% and 4.8%, using IVC with two-level and three-level inverters, respectively.

6.2.7 Stator Flux and Rotor Flux Response

Stator flux response is drawn on channel 3. When the wind velocity is changed from maximum to minimum at $t=2$ s, then stator flux reduces from maximum to minimum. IVC with two-level inverter is giving stator peak flux of 0.94 pu with more settling time 0.71 s, but IVC with three-level inverter has peak flux of 0.96 pu with less settling time 0.62 s which is nearer its rated flux at maximum wind velocity of 15 m/s. Rotor flux response has been taken on channel 4. At 15 m/s of wind velocity, rotor peak flux and more settling time have been found of 0.93 pu and 0.69 s with IVC using a two-level inverter, but IVC using three-level inverter yields rotor peak flux of 0.962 pu with less settling time 0.56 s.

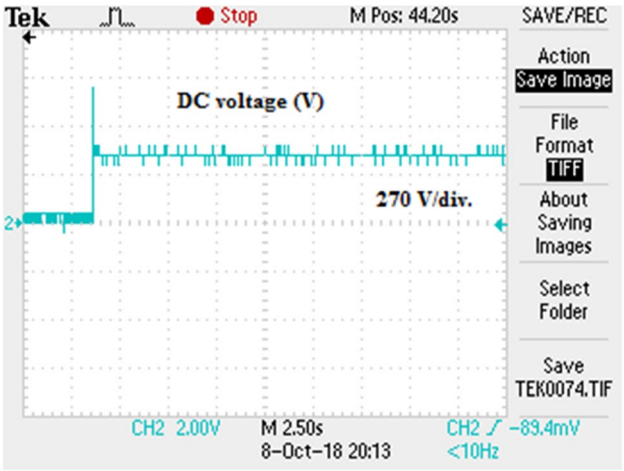

Fig. 34 DC voltage with TLI

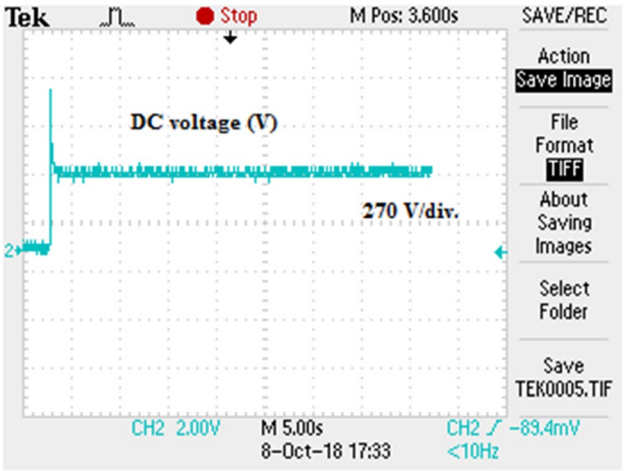

Fig. 35 DC voltage with MLI

6.2.8 DC Voltage Response

DC voltage response is discussed in Figs. 34 and 35. Reference DC voltage is selected as 400 V. At $t = 2$ s, wind speed is reduced from 15 to 9 m/s and then IVC with two-level inverter gives DC voltage undershoot of 1.77% and settles within 0.72 s, but IVC with three-level inverter has undershoot of 1.27% and settles within 0.64 s only. IVC with a three-level inverter yields better dynamic response compared with a two-level inverter. The comparisons between simulation and experimental results with IVC using two-level and three-level inverters are tabulated in Table 2. The experimental results validate the simulation results.

7 Conclusion

The limitation of self-excited induction generator (SEIG) when used in the stand-alone wind energy system (WES) is of poor voltage regulation at variable speed. The indirect vector control technique is employed for both the generator side converter (GSC) and load side converter (LSC) to regulate the variation of SEIG speed, DC link voltage, and electromagnetic torque independently. The space vector pulse width modulation (SVPWM) strategy is employed in the wind energy system. Two-level and three-level space vectors PWM inverter are chosen. The two-level load side inverter (TLI) is replaced by a three-level neutral point clamped multilevel inverter to overcome the harmonics profile of output voltage. Moreover, the proposed IVC technique with a three-level inverter scheme is also found to be much better in comparison with a two-level inverter. Hybrid control technique with MLI scheme can be explored at variable speed operation of induction generator for future work.

Table 2 Simulation and experimental results comparison of TLI and MLI

Parameters	Properties	Simulation results TLI/MLI	Experimental results TLI/MLI
SEIG speed	Undershoot/overshoot %	4.57/4	6/5
	Settling time(s)	0.73/0.6	0.75/0.6
DC voltage	Undershoot/overshoot %	1.75/1.25	1.77/1.27
	Settling time(s)	0.70/0.62	0.72/0.64
Electromagnetic torque	Undershoot/overshoot %	2.7/1.33	3/2
	Settling time(s)	0.74/0.69	0.77/0.71
Stator current	THD%	7.41/6.06	9.3/7.2
Stator voltage	THD%	4.95/2.95	7.3/4.8

Appendix

Parameters of induction machine	Parameters of IGBT inverter	Parameters of converter
$P = 4000$ W	$R_{on} = 1$ mΩ	$R_{on} = 0.001$ Ω
$V = 400$ V	$R_S = 105$ Ω	$V_f = 0.8$ V
$f = 50$ Hz		$L_{on} = 1$ mH
$R_S = 0.035$ pu		
$N = 1430$ rpm		
$H.P = 5.4$		
$Ll_s = 0.045$ pu		

Acknowledgements The current work is supported by the Ministry of Human Resource Development, Government of India, through a Ph.D. scholarship grant.

References

1. Chatterjee, S.; Chatterjee, S.: Review on the techno-commercial aspects of wind energy conversion system. IET Renew. Power Gener. Rev. **12**(14), 1581–1608 (2018)
2. Sener, S.E.C.; Sharp, J.L.; Anctil, A.: Factors impacting diverging paths of renewable energy: a review. Renew. Sustain. Energy Rev. **81**, 2335–2342 (2019)
3. Xu, J.; Li, L.; Zheng, B.: Wind energy generation technological paradigm diffusion. Renew. Sustain. Energy Rev. **59**, 436–449 (2016)
4. Li, Z.; Wong, S.-C.; Tse, C.K.; Liu, X.: Controller saturation nonlinearity in doubly fed induction generator- based wind turbines under unbalanced grid conditions. Int. J. Circuit Theory Appl. **44**(8), 1–18 (2015)
5. Dewangan, S.; Dyanamina, G.; Kumar, N.: Performance improvement of wind-driven self-excited induction generator using fuzzy logic controller. Int. Trans. Elect. Energy Syst. **29**(8), 1–20 (2019)
6. Ko, D.H.; Jeong, S.T.; Kim, Y.C.: Assessment of wind energy for small-scale wind power in Chuuk State, Micronesia. Renew. Sustain. Energy Rev. **52**, 613–622 (2015)
7. Saha, S.; Haque, M.E.; Mahmud, M.A.: Diagnosis and mitigation of sensor malfunctioning in a permanent magnet synchronous generator based wind energy conversion system. IEEE Trans. Energy Conv. **33**(3), 938–948 (2018)
8. Chandramohan, K.; Padmanaban, S.; Kalyanasundaram, R.; Blaabjerg, F.: Modeling of five-phase, self-excited induction generator for wind mill application. Elect. Power Comp. Syst. **46**(3), 353–363 (2018)
9. Ejiofor, O.S.; Candidus, E.U.; Victory, M.C.; Ugochukwu, E.C.: Wind energy dynamics of the separately excited induction generator. Int. J. Appl. Sci. **2**(1), 22–32 (2019)
10. Fernandes, J.F.P.; Perez-Sanchez, M.; da Silva, F.F.; Lopez-Jimenez, P.A.; Ramos, H.M.; Branco, P.J.C.: Optimal energy efficiency of isolated PAT sytems by SEIG excitation tuning. Energy Conv. Manag. **183**(1), 391–405 (2019)
11. Jha, D.; Thakur, A.: Novel control strategy for standalone wind energy conversion system supplying power to isolated DC Load. Majlesi J. Elect. Eng. **13**(1), 19–29 (2019)
12. Kalla, U.K.; Singh, B.; Murthy, S.S.: Modified electronic load controller for constant frequency operation with voltage regulation of small hydro-driven single-phase SEIG. IEEE Trans. Ind. Appl. **52**(4), 2789–2800 (2016)
13. Mosaad, M.I.: Model reference adaptive control of STATCOM for grid integration of wind energy systems. IET Elect. Power Appl. **12**(5), 605–613 (2018)
14. Chilipi, R.R.; Singh, B.; Murthy, S.S.: Performance of a self-excited induction generator with DSTATCOM-DTC drive-based voltage and frequency controller. IEEE Trans. Energy Conv. **29**(3), 545–557 (2014)
15. Chauhan, P.J.; Chatterjee, J.K.: A Novel speed adaptive stator current compensator for voltage and frequency control of standalone SEIG feeding three-phase four-wire system. IEEE Trans. Sustain. Energy **10**(1), 248–256 (2019)
16. Arthishri, K.; Kumaresan, N.; Gounden, N.A.: Analysis and application of three-phase SEIG with power converters for supplying single-phase grid from wind energy. IEEE Syst. J. **13**(2), 1813–1822 (2019)
17. dos Santos, T.H.; Goedtel, A.; da Silva, S.A.O.; Suetake, M.: Scalar control of an induction motor using a neural sensorless technique. Elect. Power Syst. Res. **108**, 322–330 (2014)
18. Jaladi, K.K.; Sandhu, K.S.: DC-link transient improvement of SMC-based hybrid control of DFIG-WES under asymmetrical grid faults. Int. Trans. Elect. Energy Syst. **28**(12), 1–27 (2018)
19. Jaladi, K.K.; Sandhu, K.S.: A new hybrid control scheme for minimizing torque and flux ripple for DFIG-based WES under random change in wind speed. Int. Trans. Elect. Energy Syst. **29**(4), 1–15 (2019)
20. Bašić, M.; Vukadinović, D.; Grgić, I.: Compensation of stray load and iron losses in small vector-controlled induction generators. IEEE Trans. Energy Conv. **1**, 9 (2019)
21. Baˇ, M.; Vukadinović, D.: Online efficiency optimization of a vector controlled self-excited induction generator. IEEE Trans. Energy Conv. **31**(1), 373–380 (2016)
22. Pal, A.; Das, S.; Chattopadhyay, A.K.: An improved rotor flux space vector based MRAS for field oriented control of induction motor drives. IEEE Trans. Power Elect. **33**(6), 5131–5141 (2018)
23. Chinmaya, K.A.; Singh, G.K.: Performance evaluation of multiphase induction generator in stand-alone and grid-connected wind energy conversion system. IET Renew. Power Gener. **12**(7), 823–831 (2018)
24. Tatte, Y.N.; Aware, M.V.: Torque ripple and harmonic current reduction in a three-level inverter-fed direct-torque-controlled five-phase induction motor. IEEE Trans. Ind. Elect. **64**(7), 5265–5275 (2017)
25. Maswood, A.I.; Gabriel, O.H.P.; Al, A.E.: Comparative study of multilevel inverters under unbalanced voltage in a single DC link. IET Power Elect. **6**(8), 1530–1543 (2013)
26. Azeem, H.; Yellasiri, S.; Jammala, V.; Naik, B.S.; Panda, A.K.: A Fuzzy logic based switching methodology for a cascaded H-bridge multi-level inverter. IEEE Trans. Power Elect. **34**(10), 9360–9364 (2019)
27. Boulouiha, H.M.; Allali, A.; Laouer, M.; Tahri, A.; Denaï, M.; Draou, A.: Direct torque control of multilevel SVPWM inverter in variable speed SCIG-based wind energy conversion system. Renew. Energy **80**, 140–152 (2015)
28. Bandy, K.; Stumpf, P.: Model predictive torque control for multilevel inverter fed induction machines using sorting networks. IEEE Access **9**, 13800–13813 (2021)
29. Xiao, D.; Alam, K.S.; Osman, I.; Akter, M.P.; Shakib, S.M.S.I.; Rahman, M.F.: Low complexity model predictive flux control for three-level neutral-point clamped inverter-fed induction motor drives without weighting factor. IEEE Trans. Ind. Appl. **56**(6), 6496–6506 (2020)